Clim. Past Discuss., 9, 4475–4498, 2013
www.clim-past-discuss.net/9/4475/2013/
doi:10.5194/cpd-9-4475-2013


Climate of the Past Discussions
Open Access



# Low-latitude climate variability in the Heinrich frequency band of the Late Cretaceous Greenhouse world

**N. J. de Winter, C. Zeeden, and F. J. Hilgen**

Department of Earth Sciences, Faculty of Geosciences, Utrecht University, Budapestlaan 4, 3584 CD Utrecht, the Netherlands

Received: 30 May 2013 – Accepted: 21 June 2013 – Published: 8 August 2013

Correspondence to: N. J. de Winter (niels_de_winter@live.nl)

Published by Copernicus Publications on behalf of the European Geosciences Union.







## Abstract

Deep marine successions of early Campanian age from DSDP site 516F drilled at low paleolatitudes in the South Atlantic reveal distinct sub-Milankovitch variability in addition to precession and eccentricity related variations. Elemental abundance ratios point to a similar climatic origin for these variations and exclude a quadripartite structure – as observed in the Mediterranean Neogene – of the precession related cycles as an explanation for the inferred semi-precession cyclicity in MS. However, the semi-precession cycle itself is likely an artifact, reflecting the first harmonic of the precession signal. The sub-Milankovitch variability is best approximated by a ~ 7 kyr cycle as shown by spectral analysis and bandpass filtering. The presence of sub-Milankovitch cycles with a period similar to that of Heinrich events of the last glacial cycle is consistent with linking the latter to low-latitude climate change caused by a non-linear response to precession induced variations in insolation between the tropics.

## 1 Introduction

The origin of sub-Milankovitch climate variability with periods between 5 and 15 kyr (e.g., Hagelberg et al., 1994) remains elusive and is far less understood than cycles – directly – related to the orbital climate forcing. So-called Heinrich-events of the last glacial cycle from the North Atlantic (Heinrich, 1988; Bond et al., 1992; Hemming, 2004) represent the best known and most widely studied case of sub-Milankovitch variability, although variability on this time scale has been described from older glacials of the last 2.5 Myr as well (Becker et al., 2006 and references therein). Heinrich events denote rapid and massive discharges of icebergs into the North Atlantic during the last glacial cycle, suggesting that ice sheets are either directly responsible for or amplify an initial climate signal. They were first described by Heinrich (1988), who linked these to low-latitude climate to explain their recurrence time of ~ 7–8 kyr. On the contrary, MacAyeal (1993) held internal ice sheet oscillations responsible for their formation, while other





CPD
9, 4475–4498, 2013



autogenic models favor amplified jökulhlaupt events (Johnson and Lauritzen, 1995) or ice shelf instability (Hulbe, 1997; see also Hemming, 2004). They were related to white noise stochastic forcing with a magnitude similar to – random – changes in insolation of $\geq 0.5\,W\,m^{-2}$ by Hyde and Crowley (2002).

However, it cannot be excluded that such internal or stochastic events are phase locked with initial external climate changes that act on the same time scale. Indeed, other studies involved an external climatic forcing to explain instability of fringing ice shelves (Hulbe et al., 2004) linked to precession paced variations in El Nino-Southern Oscillation (ENSO) intensity in the Pacific (Clement et al., 1999). Following Heinrich (1988), a low-latitude origin of Heinrich events was favoured by McIntyre and Molfino (1996), who studied late Pleistocene abundance variations in the coccolith species *Florisphaera profunda* in the equatorial Atlantic and related these to precession driven changes in zonal wind-driven divergence in the sub-Milankovitch frequency band at times of minimum eccentricity. Ziegler (2009) and Turner (2004) relate Heinrich events to more frequent El-Niño events associated with precession induced climate variability that originates between the tropics (to explain the sub-Milankovitch periods) and is exported to higher latitudes. Moreover, several modeling studies predict sub-Milankovic-variability through nonlinear climate response (e.g. Braun et al., 2005, see also Hagelberg et al., 1994 and references therein), and numerous records (e.g. Steenbrink et al., 2003; Elrick and Hinnov, 1995; Chapman and Shackleton, 1998, 1999 and Zhao et al., 2006) indeed show such a pattern. Thus sub-Milankovitch variability has in particular been found in glacials of the last 2.5 Myr, although its origin may lie within the tropics (e.g. Hagelberg et al., 1994), suggesting that ice sheets amplify an initial (sub)orbital climate signal. Rutherford and D'Hondt (2000) suggest that $\sim 1.5$ Myr ago semi-precession cycles propagated from tropical to higher latitudes, and argue for a casual relation between semi-precession cycles, precession and eccentricity.

In case Heinrich events are related to low latitude climate change and paced by precessional forcing (and nonlinear feedback in the sub-Milankovich band), cycles with the same period may be expected from pre-Quaternary times. Such cycles have





CPD
9, 4475–4498, 2013



indeed been described from Pliocene lignite-bearing lacustrine successions of northern Greece (Steenbrink et al., 2003) and platform carbonates of the Great Bahama Bank (Reuning et al., 2006). They have further been found in fluvial floodplain successions in the Eocene Willwood Formation in North America (Abdul Aziz et al., 2008), although the latter may equally well be associated with autogenic processes acting on the floodplain (Bown and Kraus, 1993).

In the present case, a logical choice to look for the persistence of sub-Milankovitch cycles is in marine successions of Greenhouse periods of Earth history, such as the Cretaceous and Jurassic, when ice sheets are absent or play a minor role, and ice driven responses are excluded. A prime example of such climate variability comes from the marine Cretaceous (Campanian) of the South Atlantic (Park et al., 1993). They report semi-precession cycles based on time series analysis of high-resolution magnetic susceptibility records from DSDP Site 516F located at a paleolatitude of $\sim 30^{\circ}$ S. However, using magnetic susceptibility as a proxy for carbonate content does not exclude the possibility that the precession-related cycles represent sedimentary quadruplets in which the two carbonate minima, or magnetic susceptibility maxima per precession-related cycle, have a different climatic origin. Up to now, such quadruplets have only been described from the Mediterranean (e.g., de Visser et al., 1989; Hilgen et al., 2003), whereas the early South Atlantic was located at similar – but Southern Hemisphere – paleolatitudes and had a basin configuration that was comparable to the Mediterranean. Moreover, visual inspection of the magnetic susceptibility records of Park et al. (1993) reveals three rather than the expected two magnetic susceptibility maxima per precession related cycle, casting doubt on the inferred semi-precession nature of the cycles. We use XRF elemental analysis to test the potential quadruplet structure of the precession related cycles. Time series analysis is applied to examine whether these variations represent true semi-precession cycles or have a shorter period similar to that of Heinrich events.





CPD
9, 4475–4498, 2013



## 2 Geological setting

DSDP Site 516 was drilled during Leg 72 at 30°16.59′ S latitude and 35°17.10′ W longitude, in a waterdepth of more than 1300 m on the Rio Grande Rise in the South Atlantic (Barker et al., 1983). This Site was the shallowest drilled during DSDP Leg 72 and was designated for the study of upper water column characteristics of the southwestern Atlantic during the Neogene/Quaternary and late Cretaceous; sediments deposited in deeper water were recovered at other Sites. Hydraulic piston coring provided the base for detailed studies of astronomically induced climate forcing during the Quaternary and Miocene, while the Eocene/Oligocene and Cretaceous/Paleogene boundaries were targeted in rotary drilled carbonate rich successions.

Site 516 was located at a paleolatitude of ∼ 30° S during the Campanian (72.1–83.6 Ma; Gradstein et al., 2012), the time interval of interest here. At that time, the South Atlantic Ocean was a smaller, more confined ocean basin compared to the present day situation.

## 3 Methods

Samples of ∼ 1.5 cm length (∼ 12 $cm^3$; quarter cores) were taken at a spacing of ∼ 1.5 cm from DSDP Leg 72 Site 516F. Sections 5 (81–150 cm) and 6 (0–93 cm) were sampled from core 113 and Section 1 (0–135 cm) from core 114. This results in a set of 198 core samples. No continuous splice is available for DSDP Site 516. A composite of cores 113 and 114 was created by connecting these cores directly.

Samples were weighted using a Mettler P1210. A Niton XLi XRF (X-Ray-Fluorescence) Analyzer at Utrecht University was used to measure elemental abundances of the samples. Sawed down-core surfaces of samples were used for XRF measurements. The magnetic susceptibility of the samples was measured using a KLY-2 Kappabridge. A KONICA MINOLTA CM-600d spectrophotometer was used to measure color reflectance of the core samples and core surface directly at the BCR (Bremen





CPD
9, 4475–4498, 2013



Core Repository) at the MARUM, Bremen. The sampled interval for color measurements is longer than that for other measurement techniques, because some of the color data were generated directly from the core surfaces where no samples were taken. Due to cracks in the cores no equal spacing was possible for the color measurements.

Analyseries version 1.1 (Paillard et al., 1996) is used for Blackman–Tukey spectral analysis and Gaussian bandpass filtering. In addition, point moving averages (pma) of the $L^*$, $a^*$, magnetic susceptibility (MS) and XRF records were calculated to reduce noise; this results in a smoothed data set.

## 4 Results

### 4.1 Long color record

At Site 516F, color was measured with a resolution of ~ 1.5 cm in the interval between 1145 and 1166 meters composite depth (mcd). The lightness ($L^*$) and redness ($a^*$) records are shown in Fig. 1. The $L^*$ record reveals marked shifts to low values, with minima located approximately 50 cm apart. These well-defined minima occur in bundles of 3–5, with approximately 2.5 m between bundles. Moreover, three intervals (145–147, 152–156 and 159–163 mcd) can be recognized in which the $L^*$ values reach most extreme minima. These intervals can also easily be recognized when a 30 point moving average (pma) is used. Higher frequency variations can be observed throughout the $L^*$ record as well, with one or two additional, usually less distinct, minima in between the well-defined minima of the ~ 50 cm cycle.

The $a^*$ record follows a different pattern with less marked (bundling of) peaks, and a trend towards higher values before returning to lower values in the top 4–5 m (Fig. 1b). The interval from 1145 to 1150 mcd reveals three distinct shifts to lower values. These follow a saw tooth pattern, marked by an abrupt change to minimum values followed by a gradual return to normal values interrupted by higher frequency variations. This is





CPD
9, 4475–4498, 2013



succeeded by an interval marked by minima that are ~ 90 cm apart, and an interval (up to 1156 mcd) in which the maxima are separated by ~ 50 cm and, thus, more closely spaced together. The uppermost interval marked by a return to negative values shows a less regular pattern and less pronounced variations.

The $L^*$ spectrum (Fig. 2) reveals a marked double peak (of ~ 43 and 53 cm) that corresponds to the ~ 50 cm cycle, which reflects the prominent shifts to minimum values observed in the long record. The bandpass filtered component of this cycle, including both spectral peaks, is shown in Fig. 1. This filtered component reveals marked amplitude changes that track the grouping of this cycle in bundles described above. The $L^*$ spectrum in addition reveals less distinct peaks centered around ~ 1 and ~ 2.5 m. The latter is depicted as filtered component as an overlay on the $L^*$ record in Fig. 1. This cycle follows in part the bundling of the ~ 50 cm cycle and the associated amplitude changes of the extracted ~ 50 cm cycle (Fig. 1). Finally, spectral peaks occur with periods of around half and one third of that of the ~ 50 cm cycle.

The $a^*$ spectrum also shows a double peak around 50 cm (about 45 and 49 cm). The filtered component of this cycle is shown (Fig. 1b); as expected, this component is in anti-phase with the filtered ~ 50 cm $L^*$ cycle, with $a^*$ maxima corresponding to $L^*$ minima. In contrast to $L^*$, the $a^*$ spectrum does not reveal a 2.5 m cycle, but rather well-defined ~ 90 cm and ~ 1.6 m cycles. The extracted components of these cycles are shown in Fig. 1 as well. Finally, the $a^*$ spectrum contains peaks that correspond to approximately half the thickness of the ~ 50 cm cycle.

### 4.2 Short color, elemental abundance and MS records

Color, magnetic susceptibility and elemental records of the two selected intervals are shown in Fig. 3. The MS spectrum (Fig. 4) reveals a distinct ~ 41 cm peak as well as peaks consistent with ~ 21 and 14 cm cycles that reflect the higher frequency variations in MS. The MS record of both intervals reveals well defined maxima associated with the ~ 40–50 cm cycle (of the long interval) with higher frequency variations in between (Fig. 3). This 40–50 cm cycle follows a saw tooth pattern with an abrupt shift to the





CPD
9, 4475–4498, 2013



prominent maximum, in several cases followed upcore by two less distinct peaks of decreasing amplitude associated with the higher frequency variability. The bandpass filtered 50 cm cycle from the $L^*$ data picks up the prominent MS maxima, while the filtered 16 cm cycle (also from $L^*$ data) traces most of the observed higher frequency variability. The filtered 22 cm cycle recognizes the distinct MS maxima of the 50 cm cycle and places an extra cycle in between some of these maxima (see Fig. 5a).

The same cycles are also recognized in the $L^*$ record and spectrum (Figs. 2 and 5b), with $L^*$ minima corresponding to MS maxima, but the saw tooth pattern in MS is less clearly seen in $L^*$. The $a^*$ record and spectrum also show the ~ 50 cm cycle, but the shorter period cycles are not readily observed in the $a^*$ record and spectrum.

Elemental abundance records follow the distinct pattern observed in the MS record, presumably as a consequence of the closed sum effect of Al (and Ca; Fig. A1). We examined the elemental data as ratio over Al to eliminate this effect and reveal changes relative to terrestrial input, represented by e.g. Al (Figs. 3 and A2). Elemental data of Zr, Ti and Fe (over Al) are positively correlated with Al and MS variations associated with the 42 and 16 cm cycles. This implies that they show a relative increase compared to Al (and MS) maxima in these cycles. On the other hand, Sr, Si and Ba (over Al) show a negative correlation with Al and MS variations in these cycles (Figs. 3 and A2).

Elemental ratio spectra all reveal apparent periodicity with a cycle thickness between ~ 42 and 55 cm. This is the same cycle as observed in the $a^*$, $L^*$ and MS spectra. Like the $L^*$ and MS data, elemental ratio spectra often reveal the ~ 22 cm and ~ 16 cm period cycles as well, but less distinct.

## 5 Discussion

### 5.1 Quadruplets and semi-precession

The ~ 2.50 m and ~ 50 cm cycles, which are evident from visual inspection and spectral analysis of the records, explain a large part of the variation in the color data (of





CPD
9, 4475–4498, 2013



the long record). The filtered 2.50 m cycle in addition traces changes in the amplitude of the filtered ~ 50 cm cycle. This is only evident in the lower part (1145–1153 mcd) of the record. This amplitude modulation of the ~ 50 cm cycle by the 2.50 m cycle and the characteristic 1 : 5 ratio between these cycles suggest that the 2.50 m cycle represents the short ~ 100 kyr eccentricity cycle, while the 40–55 cm cycle corresponds to the climatic precession cycle with a ~ 19–23 kyr period. This interpretation results in an estimated average sedimentation rate of ~ 2.3 cm/kyr and is consistent with the interpretation of Park et al. (1993). In addition, a long period cycle with a thickness of 8–10 m can be recognized in the $L^*$ record of the long interval. This cycle likely corresponds to long ~ 405 kyr eccentricity. These ~ 100 and 405 kyr cycles are well expressed by the 30 pma of $L^*$ (Fig. 1).

The ~ 90 cm cycle in the $a^*$ spectrum may correspond to double precession or, more likely, to obliquity. In that case, the 1.6 m $a^*$ cycle may well reflect double obliquity, as also suggested by the results of bandpass filtering (Fig. 1). The contrast in the $L^*$ and $a^*$ spectral characteristics indicates that these parameters reflect different parts of the climate system. In general the influence of obliquity is much stronger at high latitudes, but it is also found in low-latitude climate records, even at times when obliquity controlled glacials are absent and ice-driven responses can be excluded (Lourens et al., 1996). An alternative explanation is a link to inter-hemispheric low-latitude insolation gradients that control monsoonal activity (Rossignol-Strick, 1983; Lourens and Reichart, 1996; Leuschner and Sirocko, 2003). On the other hand, results of climate modeling of orbital extremes indicate that obliquity may exert a noticeable influence on low-latitude climate systems, such as the African monsoon, through teleconnections with high-latitude insolation forcing (Tuenter et al., 2003).

The color and MS spectra of the long interval in addition reveal peaks in the sub-Milankovitch band of the spectrum. To understand this cyclicity, the selected short intervals were studied in greater detail using geochemical elements as additional proxy data. Sub-Milankovitch variations are particularly evident in MS, but are also recognized in color and elemental over Al ratios. The thicknesses of these sub-Milankovitch





CPD
9, 4475–4498, 2013



cycles (16 and 22 cm) can be translated into periods of ∼ 7 and 10 kyr, using the inferred sedimentation rate, based on a thickness of ∼ 40–55 cm for the precession related cycles combined with an average duration of ∼ 20 kyr for precession at 90 Ma (Berger et al., 1992).

Elemental ratios such as Ti/Al and Zr/Al follow the pattern of the sub-Milankovitch variations observed in MS within a precession related cycle (Fig. 3), pointing to a similar source of the terrigenous material. This observation excludes a quadripartite structure of the precession related cycles as a possible explanation for the inferred semi-precession cyclicity in MS of Park et al. (1993). Up to now, quadripartite precession related cycles with two carbonate minima/maxima per cycle having a *different* climatic origin have only been described from the Mediterranean Neogene (e.g., de Visser et al., 1989; Hilgen et al., 2003). In this case, the basic precession related cycle reveals two carbonate (and MS) maxima per cycle, but terrigenous elements over Al (e.g., Ti/Al) reveal a single cyclic variation associated with the basic cycle itself (de Visser et al., 1989; van Os et al., 1994). This points to two different sources of the terrigenous material (fluvial vs. eolian), and a precession related variation in their relative contribution associated with the relative humid and arid phase of the cycle (Foucault and Mélières, 2000), while diagenetic unmixing of carbonate plays a role as well (van Os et al., 1994). Such a quadripartite explanation is further inconsistent with the presence of three MS maxima in well-defined precession related cycles at DSDP Site 516F and their associated 16 cm (∼ 7 kyr) peak in the power spectra.

However, the latter is also in contradiction with a semi-precession origin of the sub-Milankovitch variability inferred by Park et al. (1993), as this would imply two MS maxima per cycle separated by 10–11 kyr (i.e., half a precession cycle). Such a semi-precession cycle was suggested by the results of their spectral analysis, which are confirmed by our results. However, the filtered semi-precession component alternately picks up successive prominent precession related maxima in MS, but intermediate semi-precession cycles do not pick up sub-Milankovitch variability in between the prominent MS maxima. This poor fit shows that the semi-precession cycle can best be





CPD
9, 4475–4498, 2013



explained as an artifact of the spectral analysis, reflecting the first harmonic of the precession related cyclicity rather than a cycle on its own (see also Herbert, 1994). In fact, the observed sub-Milankovitch variations are much better approximated by the ~ 7 kyr cycle (Figs. 3, 5). As a consequence, this 7 kyr (16 cm) cycle represents a real cycle as it describes the sub-Milankovitch variability observed in the proxy records. It is this cycle that is responsible for the observed triple peak signature of the most prominent precession related cycles in the short intervals.

### 5.2 Sub-Milankovitch variations in the Heinrich frequency band

As the ~ 7 kyr cycle represents the actual sub-Milankovitch cycle in the DSDP Site 516F proxy records, a climatic interpretation for this cycle is needed. The most logical explanation is to link this cycle to the influence of climatic precession between the tropics, as this would most easily explain the period shorter than that of precession in the sub-Milankovitch frequency band. At the equator, the two overhead passages of the Sun per precession cycle (during the vernal and autumnal equinoxes) lead to two insolation maxima separated by half a precession cycle (Berger et al., 2006). This would explain a semi-precession cycle, but not the ~ 7 kyr cycle. Berger et al. (1997) further investigated the amplitude of the seasonal cycle at the equator; the resulting spectrum reveals peaks associated with the semi-precession and quarter-precession components in addition to peaks associated with eccentricity (dominant) and obliquity (but not precession). In this way, a 5–6 kyr cycle can be explained, but again not a 7–8 kyr cycle. The influence of semi-precession and quarter-precession has been detected in paleoclimatic records both of the Pleistocene as well as older time intervals (e.g., Ferretti et al., 2010; Hernandez-Almeida et al., 2012; Steenbrink et al., 2003; Anderson, 2011). A possible clue to the origin of the 7–8 kyr cycle may come from simulations of sub-Milankovitch climate variability associated with dynamic vegetation, using transient climate model runs (Tuenter et al., 2007). In the model of Tuenter et al. (2007), these variations result from the dynamic vegetation response to precession forcing. For instance the monsoonal run-off reveals semi-precession and quarter-precession periods





CPD
9, 4475–4498, 2013



in runs with interactive vegetation. However, in several instances, also periods in between 10–12 and 5–6 kyr are found. For instance, the July run-off originating from the modeled Asian Monsoon shows three peaks in a precession cycle that are ∼ 7 kyr apart (Fig. 9c in Tuenter et al., 2007). This fits the climatic interpretation of the ∼ 7 kyr cycles at Site 516F as they are also recorded in elemental abundance ratios such as Ti/Al and Zr/Al, suggesting that they result from terrestrial sediment input via fluvial run-off into the paleo South Atlantic Ocean (see also Park et al., 1993). Tuenter et al. (2007) also report changes in salinity as a result of the changes in runoff, particularly in semi-enclosed basins that may be considered as an analogue for the Paleo-Atlantic Ocean. As the paleolatitude of DSDP Site 516 is at latitudes most likely influenced by trade winds, large drylands in the African hinterland may interact with vegetation in a similar way as described by Tuenter et al. (2007). However, the transient climate simulations should be repeated using more sophisticated climate–vegetation models, as an artifact related to the limited number of vegetation cannot fully be excluded.

The ∼ 7 kyr period of the sub-Milankovitch cycle at Site 516F fits the recurrence time of Heinrich events (massive input of ice-rafted debris in the North Atlantic) of the last glacial cycle remarkably well. Cycles with similar periods are not restricted to the last glacial, but are also found in $\delta^{18}$O and other proxy records of marine isotope stages (MIS) 96–100 at ∼ 2.4 Ma (Becker et al., 2005, 2006), although these lack the typical Heinrich event signature (Bond et al., 1992; results ODP Leg 162/171 IODP 303). Our observation is in agreement with the interpretation of Heinrich events being controlled by low-latitude climate changes induced by a nonlinear response to the precession cycle between the tropics. Changes in monsoonal controlled run-off on sub-Milankovitch time scales will alter salinities in the Atlantic and, hence, affect the meridional mass transport to high-latitudes. Sub-Milankovitch cycles with a similar period were also detected in laminae thickness counts of Permian evaporites (Anderson, 1982, 2011). For these cycles (as well the recorded semi- and quarter-precession cycles), a similar monsoonal origin is inferred, confirming that these originate at low-latitudes.





CPD
9, 4475–4498, 2013



## 6 Conclusions

Based on a high resolution magnetic susceptibility analysis along with XRF data and color measurements it can be concluded that no 10–11 kyr semi-precession cycle is present in DSDP Site 516F cores 113 and 114. Due to the similar chemical signature of the sub-Milankovitch cyclicity, the presence of a quadruplet structure of the precession related cycles is unlikely. The spacing between the peaks in magnetic susceptibility, color and terrestrial elements suggests a shorter 7–8 kyr sub-Milankovitch cycle as a cause for the double peaks observed by Park et al. (1993). The observation of this 7–8 kyr cycle in a low latitude Cretaceous greenhouse setting is in agreement with earlier claims that sub-Milankovitch cyclicity, associated with the marine isotope stages and so-called Heinrich events, is exported to higher latitudes from equatorial areas. This sub-Milankovitch cyclicity is assumed to be a result of nonlinear response to orbital forcing in lower latitudes, possibly related to a slow response of vegetation to changes in insolation (Tuenter et al., 2007).

*Acknowledgements.* The research leading to these results has received funding from the [European Community's] Seventh Framework Programme [FP7/2007-2013] under grant agreement no. [215458]. This research used data provided by IODP; funding was provided by NWO. We thank Walter Hale and Alex Wülbers (BCR) for core handling and hands-on support during sampling.

## References

Anderson, R. Y.: A long geoclimatic record from the Permian, J. Geophys. Res., 87, 7285–7294, 1983.

Anderson, R. Y.: Enhanced climate variability in the tropics: a 200 000 yr annual record of monsoon variability from Pangea's equator, Clim. Past, 7, 757–770, doi:10.5194/cp-7-757-2011, 2011.

Aziz, A. H., Hilgen, F. J., van Luijk, G. M., Sluijs, A., Kraus, M. J., Pares, J. M., and Gingerich, P. D.: Astronomical climate control on paleosol stacking patterns in the upper Pa-





CPD
9, 4475–4498, 2013



leocene – lower Eocene Willwood Formation, Bighorn Basin, Wyoming, Geology, 36, 531–534, 2008.
Barker, P. F., Carlson, R. L., Johnson, D. A., et al.: Shipboard Scientific Party: Site516: Rio Grande Rise, in: Init. Repts. DSDP, 72, edited by: Barker, P. F., Carlson, R. L. and Johnson, D. A., US Govt. Printing Office, Washington, 155–338, 1983.
Becker, J., Lourens, L. J., Hilgen, F. J., van der Laan, E., Kouwenhoven, T. J., and Reichart, G.: Late Pliocene climate variability on Milankovitch to millennial time scales: a high-resolution study of MIS100 from the Mediterranean, Palaeogeogr. Palaeoclim., 228, 338–360, 2005.
Becker, J., Lourens, L. J., and Raymo, M. E.: High-frequency climate linkages between the North Atlantic and the Mediterranean during marine oxygen isotope stage 100 (MIS100), Paleoceanography, 21, PA3002, doi:10.1029/2005PA001168, 2006.
Berger, A. and Loutre, M. F.: Intertropical latitudes and precessional and half-precessional cycles, Science, 278, 1476–1478, 1997.
Berger, A., Loutre, M. F., and Laskar, J.: Stability of the astronomical frequencies over the Earth's history for paleoclimate studies, Science, 255, 560–566, 1992.
Berger, A., Loutre, M. F., and Mélice, J. L.: Equatorial insolation: from precession harmonics to eccentricity frequencies, Clim. Past, 2, 131–136, doi:10.5194/cp-2-131-2006, 2006.
Bond, G., Heinrich, H., Broecker, W., Labeyrie, L., McManus, J., Andrews, J., Huon, S., Janitschik, R., Clasen, S., Simet, C, Tedesco, K., Klas, M., Bonani, G., and Ivy, S.: Evidence for massive discharge of icebergs into the North Atlantic ocean during the last glacial period, Nature, 360, 245–249, 1992.
Bown, T. M. and Kraus, M. J.: Time-stratigraphic reconstruction and integration of paleopedologic, sedimentologic, and biotic events (Willwood Formation, Lower Eocene, Northwest Wyoming, USA), Palaios, 8, 68–80, 1992.
Braun, H., Christl, M., Rahmstorf, S., Ganopolski, A., Mangini, A., Kubatzki, C., Roth, K., and Kromer, B.: Possible solar origin of the 1,470-year glacial climate cycle demonstrated in a coupled model, Nature, 485, 208–211, 2005.
Chapman, M. R. and Shackleton, N. J.: Millennial-scale fluctuations in North Atlantic heat flux during the last 150,00 years, Earth Planet. Sc. Lett., 159, 57–70, 1998.
Chapman, M. R. and Shackleton, N. J.: Global ice-volume fluctuations, North Atlantic ice-rafting events, and deep-ocean circulation changes between 130 and 70 ka, Geology, 27, 795–798, 1999.





CPD
9, 4475–4498, 2013



Clement, A. C., Seager, R., and Cane, M. A.: Orbital controls on the tropical climate, Paleoceanography, 14, 441–456, 1999.
de Visser, J. P., Ebbing, J. H. J., Gudjonsson, L., Hilgen, F. J., Jorissen, F. J., Verhallen, P. J. J. M., and Zevenboom, D.: The origin of rhythmic bedding in the Pliocene Trubi formation of Sicily, southern Italy, Palaeogeogr. Palaeoclim., 69, 45–66, 1989.
Elrick, M. and Hinnov, L. A.: Millennial-sclae climate origins for stratification in Cambrian and Devonian deep-water rhythmites, western USA, Palaeogeogr. Palaeocl., 123, 353–372, 1995.
Ferretti, P., Crowhurst, S. J., Hall, M. A., and Cacho, I.: North Atlantic millennial-scale climate variability 910 to 790 ka and the role of the equatorial insolation forcing, Earth Planet. Sc. Lett., 293, 28–41, 2010.
Foucault, A. and Mélières, F.: Paleoclimatic cyclicity in central Mediterranean Pliocene sediments: the mineralogical signal, Palaeogeogr. Palaeocl., 158, 311–323, 2000.
Gradstein, F. M., Ogg, J. G., Schmitz, M., and Ogg, G.: The Geologic Time Scale 2012, Elsevier, 1176 pp., 2012.
Hilgen, F. J., Abdul Aziz, H., Krijgsman, W., Raffi, I., and Turco, E.: Integrated stratigraphy and astrochronology of the Serravallian and lower Tortonian at Monte dei Corvi (Middle–Upper Miocene, Northern Italy), Palaeogeogr. Palaeocl., 199, 229–264, 2003.
Hagelberg, T. K., Bond, G., and deMenocal, P.: Milankovitch band forcing of sub-Milankovitch climate variability during the Pleistocene, Paleoceanography, 9, 545–558, 1994.
Heinrich, H.: Origin and consequences of cyclic ice rafting in the northeast Atlantic Ocean during the past 130,000 years, Quaternary Res., 29, 142–152, 1988.
Hemming, S. R.: Heinrich events: massive late Pleistocene detritus layers of the North Atlantic and their global climate imprint, Rev. Geophys., 42, 1–43, 2004.
Herbert, T. D.: Reading orbital signals distorted by sedimentation: models and examples, in: Orbital Forcing and Cyclic Sequences, edited by: de Boer, P. L. and Smith, D. G., Blackwell Publishing, Oxford, UK, 483–507, 1994.
Hernández-Almeida, I., Sierro, F. J., Cacho, I., and Flores, J. A.: Impact of suborbital climate changes in the North Atlantic on ice sheet dynamics at the Mid-Pleistocene Transition, Paleoceanography, 27, 1–14, 2012.
Hulbe, C. L.: An ice shelf mechanism for Heinrich layer production, Paleoceanography, 12, 711–717, 1997.





CPD
9, 4475–4498, 2013



Hulbe, C. L., MacAyeal, D. R., Denton, G. H., Kleman, J., and Lowell, T. V.: Catastrophic ice shelf breakup as the source of Heinrich event icebergs, Paleoceanography, 19, PA1004, doi:10.1029/2003PA000890, 2004.
Hyde, W. T. and Crowley, T. J.: Stochastic forcing of Pleistocene ice sheets: implications for the origin of millennial-scale climate oscillations, Paleoceanography, 17, 1067, doi:10.1029/2001PA000669, 2002.
Johnson, R. G. and Lauritzen, S.-E.: Hudson Bay-Hudson Strait jökulhlaups and Heinrich events: a hypothesis, Palaeogeogr. Palaeocl., 117, 123–137, 1995.
Lourens, L. J. and Reichart, G. J.: Low latitude forcing of glacial cycles, in: Late Quaternary variability of the Arabian Sea Monsoon and Oxygen Minimum Zone, Ph.D. thesis, Utrecht University, 1996.
Leuschner, D. C. and Sirocko, F.: Orbital insolation forcing of the Indian monsoon – a motor for global climate changes?, Palaeogeogr. Palaeocl., 197, 83–95, 2003.
MacAyeal, D. R.: Binge/purge oscillations of the Laurentide ice sheet as a cause of the North Atlantic's Heinrich events, Paleoceanography, 8, 775–784, 1993.
McIntyre, A. and Molfino, B.: Forcing of Atlantic equatorial and subpolar millennial cycles by precession, Nature, 274, 1867–1870, 1996.
Paillard, D., Labeyrie, L., and Yiou, P.: Macintosh program performs time-series analysis, EOS T. Am. Geophys. Un., 77, p. 379, 1996.
Park, J., D'Hondt, S. L., King, J. W., and Gibson, C.: Late Cretaceous precessional cycles in double time: a warm-Earth Milankovitch response, Science, 261, 1431–1434, 1993.
Pestiaux, P., van der Mersch, I., Berger, A., and Duplessy, J. C.: Paleoclimatic variability at frequencies ranging from 1 cycle per 10.000 years to 1 cycle per 1000 years: evidence for nonlinear behaviour of the climate system, Climatic Change, 12, 9–37, 1988.
Reuning, L., Reijmer, J. J. G., Betzler, C., Timmermann, A., and Steph, S.: Sub-Milankovitch cycles in periplatform carbonates from the early Pliocene Great Bahama Bank, Paleoceanography, 21, PA1017, doi:10.1029/2004PA001075, 2006.
Rossignol-Strick, M.: Mediterranean Quaternary sapropels, an immediate response of the African monsoon to variation of insolation, Palaeogeogr. Palaeocl., 49, 237–263, 1985.
Rutherford, S. and D'Hondt, S.: Early onset and tropical forcing of 100,000-year Pleistocene glacial cycles, Nature, 408, 72–75, 2000.





CPD
9, 4475–4498, 2013



Steenbrink, J., Kloosterboer-van Hoeve, M. L., and Hilgen, F. J.: Millennial-scale climate variations recorded in Early Pliocene colour reflectance time series from the lacustrine Ptolemais Basin (NW Greece), Global Planet. Change, 36, 47–75, 2003.

Tuenter, E., Weber, S. L., Hilgen, F. J., and Lourens, L. J.: The response of the African summer monsoon to remote and local forcing due to precession and obliquity, Global Planet. Change, 36, 219–235, 2003.

Tuenter, E., Weber, S. L., Hilgen, F. J., and Lourens, L. J.: Simulating sub-Milankovitch climate variations associated with vegetation dynamics, Clim. Past, 3, 169–180, doi:10.5194/cp-3-169-2007, 2007.

Turner, J.: The El Niño-Southern Oscillation and Antarctica, Int. J. Climate, 24, 1–31, 2004.

Van Os, B. J. H., Lourens, L. J., Hilgen, F. J., De Lange, G. J., and Beaufort, L.: The formation of Pliocene sapropels and carbonate cycles in the Mediterranean: diagenesis, dilution and productivity, Paleoceanography, 9, 601–618, 1994.

Zhao, M., Huang, C., Wang, C., and Wei, G.: A millennial-scale $U^{K'}_{37}$ sea-surface temperature record from the South China Sea (8° N) over the last 150 kyr: Monsoon and sea-level influence, Palaeogeogr. Palaeocl., 236, 39–55, 2006.

Ziegler, M.: Orbital forcing of the Late Pleistocene boreal summer monsoon: links to North Atlantic cols events and El Niño – Southern Oscillation Dissertation, Geologica Ultraiectina, Amsterdam, 2009.





CPD
9, 4475–4498, 2013



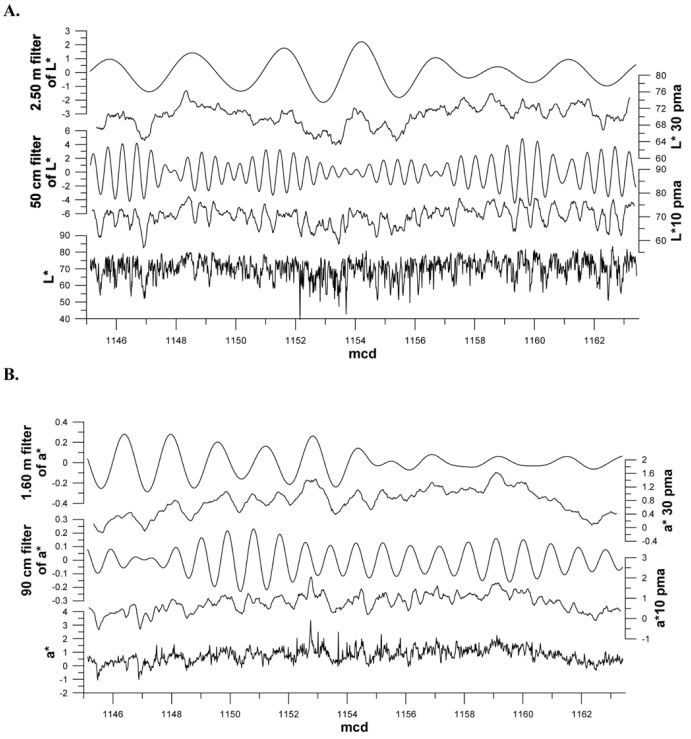


**Fig. 1.** Point moving averages of $L^*$ with filters of presumed precession and eccentricity wavelengths **(A)** and $a^*$ with filters of presumed obliquity and double obliquity wavelengths **(B)**.





CPD
9, 4475–4498, 2013



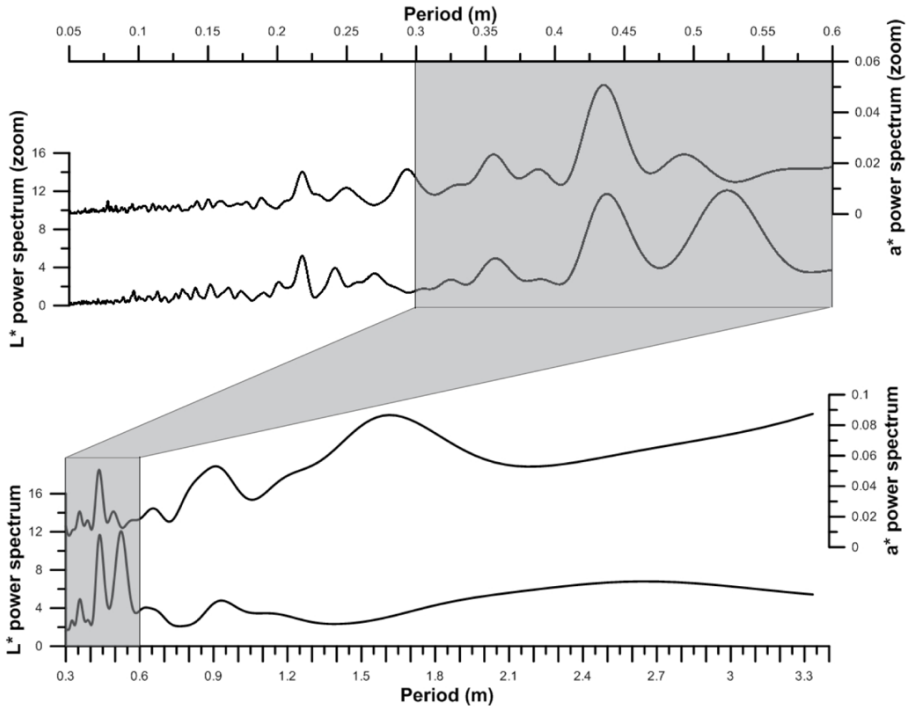


**Fig. 2.** Blackman–Tukey powerspectra of $L^*$ and $a^*$.





CPD
9, 4475–4498, 2013

Low-latitude climate variability in the Heinrich frequency band

N. J. de Winter et al.

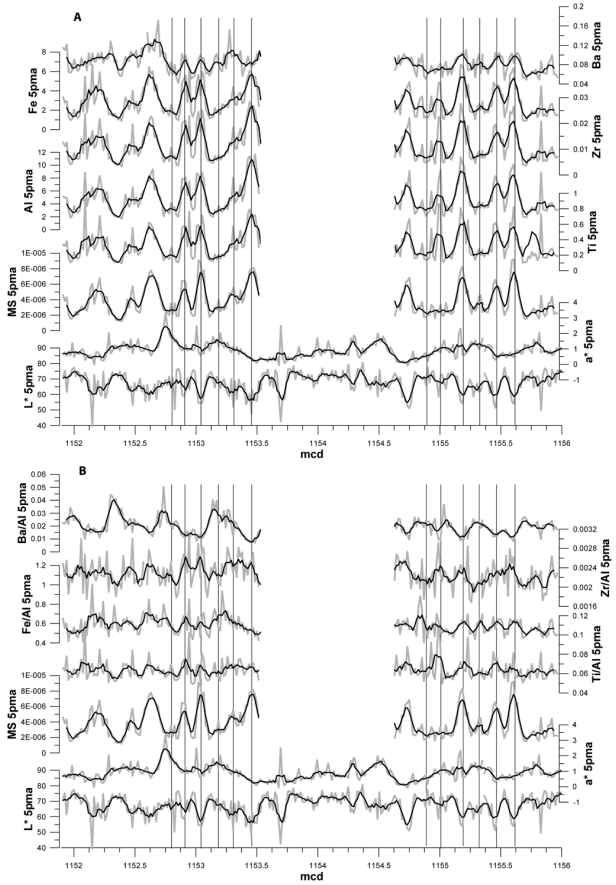


**Fig. 3.** $L^*$, $a^*$ and magnetic susceptibility short data with Ti, Fe, Zr and Ba abundances **(A)** and abundances divided by Al **(B)** plotted against depth.





CPD
9, 4475–4498, 2013

Low-latitude climate variability in the Heinrich frequency band

N. J. de Winter et al.

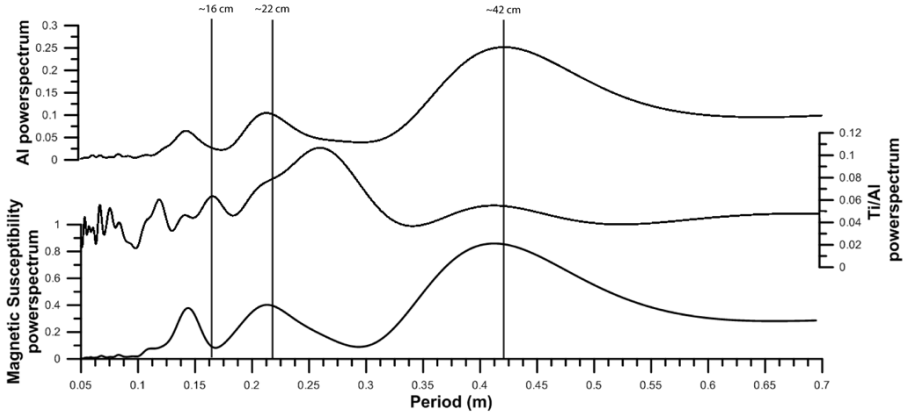


**Fig. 4.** Blackman–Tukey powerspectra of magnetic susceptibility, Ti/Al and Al.





CPD
9, 4475–4498, 2013



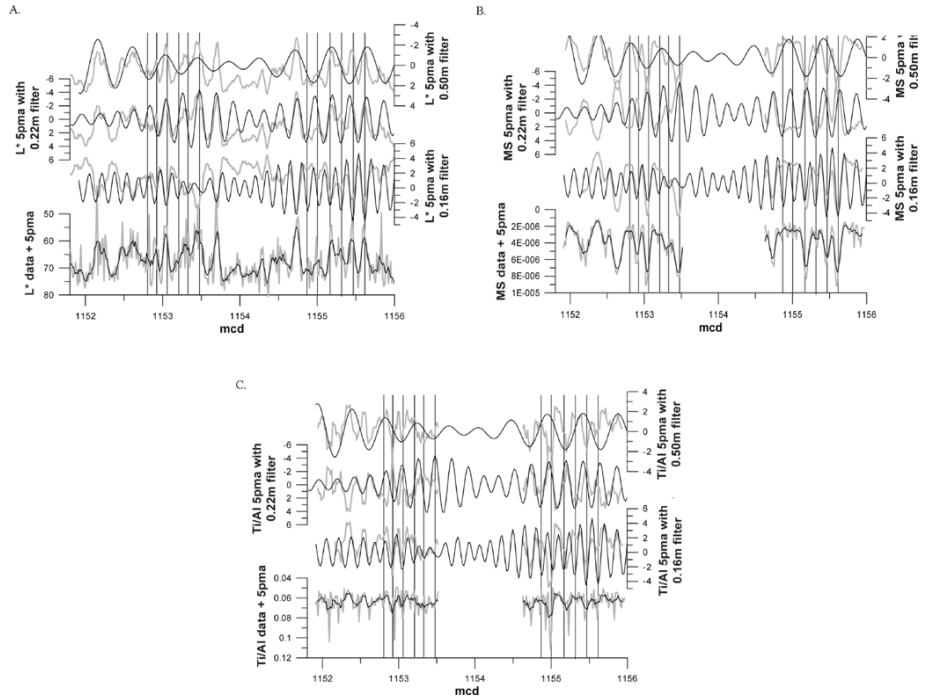


**Fig. 5.** $L^*$ **(A)**, Magnetic susceptibility **(B)** and Ti/Al **(C)** with 0.50 m, 0.22 m and 0.16 m filters of $L^*$.





CPD
9, 4475–4498, 2013

Low-latitude climate variability in the Heinrich frequency band

N. J. de Winter et al.



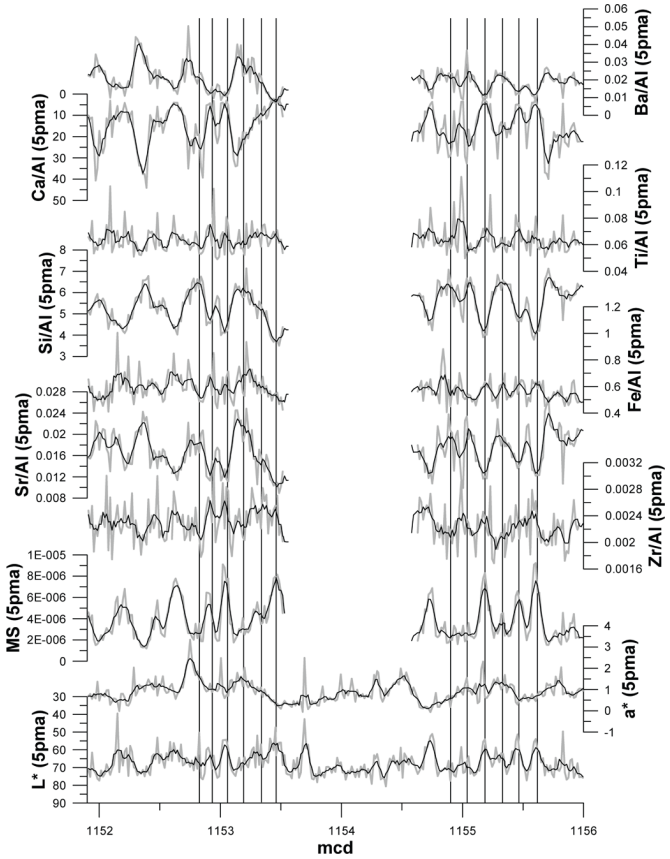


**Fig. A1.** $L^*$, $a^*$, magnetic susceptibility and all XRF elemental abundances with 5 point moving averages plotted against depth.





CPD
9, 4475–4498, 2013



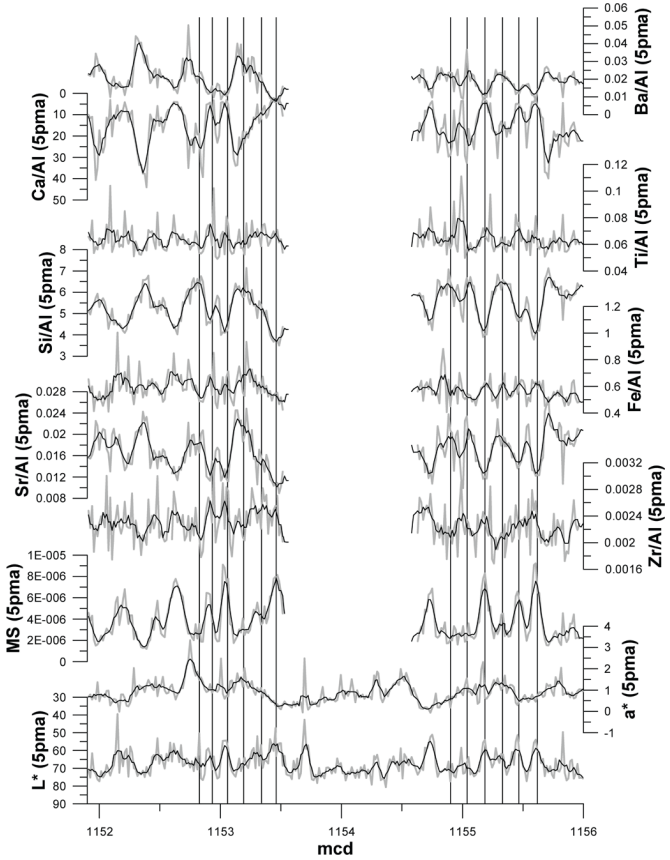


**Fig. A2.** $L^*$, $a^*$, magnetic susceptibility and all XRF elemental abundances divided by Al with 5 point moving averages plotted against depth.





CPD
9, 4475–4498, 2013

Low-latitude climate variability in the Heinrich frequency band

N. J. de Winter et al.